npg

ORIGINAL ARTICLE

The simplest route to generating a train of attosecond pulses

Kazumichi Yoshii, John Kiran Anthony and Masayuki Katsuragawa

We report on two novel routes to generating a train of attosecond pulses from a broad discrete spectrum in the near-infrared–visible–ultraviolet range. One extends an integer-temporal-Talbot (ITT) concept to include high-order spectral dispersions and generates a pulse train that completely satisfies the transform-limited condition. The other numerically explores the optimum conditions under which we can obtain an attosecond pulse train that approximately satisfies the transform-limited condition. The second method is more practical than the first. Either of these methods is extremely simple and robust; we need only to place a few thin dispersive materials in the optical path and to adjust their thicknesses without spatially dispersing the frequency components. We numerically demonstrate the generation of a train of attosecond pulses with a transform-limited pulse duration of 728 as and a repetition period of 8.03 fs in gaseous parahydrogen.

INTRODUCTION

As a result of the studies of high harmonic generation that have been extensively conducted since the 1980s and have been boosted by the matured ultrafast technology represented by the Ti:sapphire laser,[1] 'attosecond science' is flourishing.[2] Coherent attosecond laser sources[3–12] have been realized as part of this research, and on the basis of such technology, various lines of research centered on the ultrafast dynamics of electrons in atoms[3–18] or molecules[19,20] are being developed.[2] In recent years, through the powering of such attosecond laser sources,[21] nonlinear optics in the attosecond regime are also being explored.[22,23] These studies have mainly been executed in the extreme ultraviolet regime. On the other hand, in closely related studies in the near-infrared–visible–ultraviolet range, curious new approaches based on four-wave mixing in whispering-gallery-mode microresonators[24,25] or the adiabatic excitation of Raman transitions[26–39] are being extensively examined to generate broad, discrete, coherent spectra spanning over an octave and then manipulate them. Here, we discuss novel methods of generating a train of attosecond pulses by controlling such highly discrete coherent spectra. The methods are surprisingly simple and very attractive, especially because their flexibility makes them applicable over a wide range, including in high-powered lasers.

METHODS

Extended integer-temporal-Talbot (ITT) method

We introduce two independent approaches. The first approach is an extension of the ITT concept[40,41] and can be applied to ultrabroad bandwidths over petahertz (PHz). The ITT method has essentially been discussed in terms of the generation of a pulse train in the picosecond regime (spectral bandwidth: tens of GHz), mainly regarding its application to optical communications technology.

$$\Theta(\omega_m) \cong \left\{ \theta^{(0)} + \theta^{(1)} m\Delta\omega \right\} + \frac{1}{2!} \theta^{(2)} (m\Delta\omega)^2 \qquad (1)$$

The point of the idea is that in controlling dispersion to form a Fourier transform-limited (TL) pulse train, the spectral phase dispersions, $\theta^{(2)}(m\Delta\omega)^2/2!$, of all discrete spectral components, $\omega_m : (\omega_0 + m\Delta\omega)$ (ω_0, center frequency; m, integer; $\Delta\omega$, frequency space), are controlled to be integer multiples of π by adding a positive second-order dispersion (group velocity dispersion) of the materials.

The ITT method is very attractive, because it is applicable regardless of the sign of the chirp initially included in a pulse, and it does not need the special structured devices that are employed to provide negative dispersion in popular ultrashort pulse generation techniques. The ITT method can function well in cases where the spectral discreteness is fairly high ($\Delta\omega > \sim$GHz). For example, in optical communications technology, the spectral spacing is typically located in a range of tens of GHz. A standard kilometer-length optical fiber can therefore become a convenient tool for providing appropriate positive second-order dispersion using the ITT method.

The ITT method can also be applied to spectra with much wider frequency spacings. However, we encounter a limitation when the spacing reaches about 10 THz (pulse duration: tens of fs).[42] In such a situation, the high-order dispersions are not trivial and destroy the ITT condition. This difficulty can be overcome by extending the original ITT concept to include high-order dispersions.

Department of Engineering Science, University of Electro-Communications, Tokyo, Japan
Correspondence: Professor M Katsuragawa, Department of Engineering Science, University of Electro-Communications, 1–5–1 Chofugaoka, Chofu-shi, Tokyo 182–8585, Japan
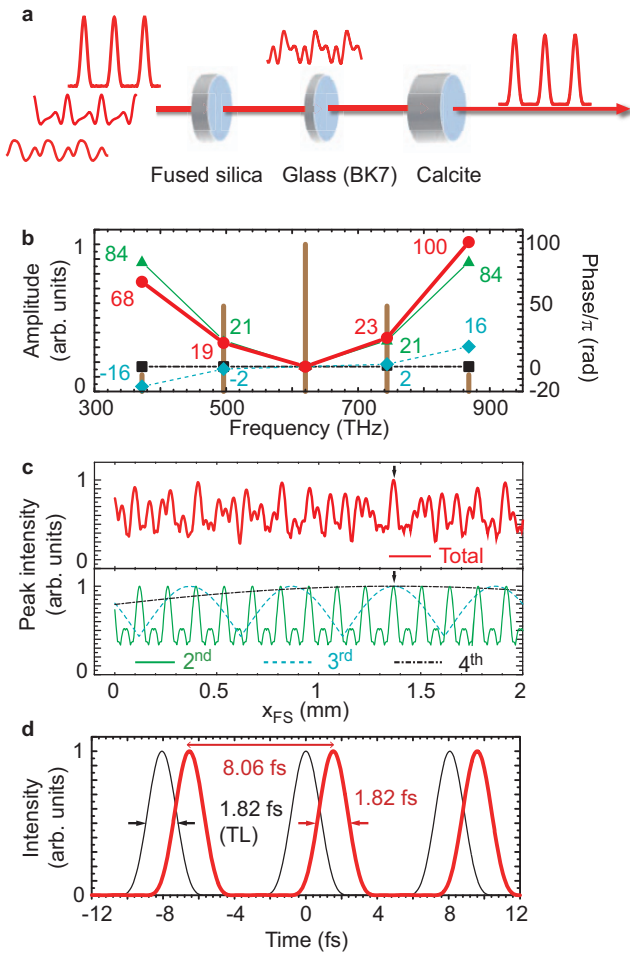E-mail: katsura@pc.uec.ac.jp

Figure 1 TL pulse generation using the extended-ITT method. (**a**) Conceptual illustration of the method. (**b**) Power spectrum and its spectral phases at the second- (thin green line), third- (dashed blue line) and fourth- (dashed and dotted black line) order dispersions and their total (red line). (**c**) Peak intensity variation of waveforms as a function of the thickness of the fused silica-glass plate. (**d**) Temporal intensity waveform created by applying the extended-ITT method (thick line).

As a typical example, we discuss a discrete spectrum (bandwidth: $2\pi\times496$ THz) consisting of five longitudinal modes with an angular frequency spacing, $\Delta\omega$, of $2\pi\times124$ THz (Figure 1b). Equation (2) expresses the spectral phase shift, $\Phi(\omega)=n(\omega)\omega x/c$, given through a dispersive material with a refractive index of $n(\omega)$ and a length of x, where c is the speed of light in vacuum and m is a longitudinal mode number from -2 to 2.

$$\Phi(\omega_m)=\left\{\phi^{(0)}x+\phi^{(1)}xm\Delta\omega\right\}+\frac{1}{2!}\phi^{(2)}x(m\Delta\omega)^2$$
$$+\frac{1}{3!}\phi^{(3)}x(m\Delta\omega)^3+\frac{1}{4!}\phi^{(4)}x(m\Delta\omega)^4 \qquad (2)$$

When the spectrum spreads across several hundreds of THz, the spectral phases are substantially influenced by material high-order dispersions (Figure 1b). Even in such cases, however, as understood from Equation (2), if the high-order dispersion terms, $\phi^{(h)}x(m\Delta\omega)^h/h!$ ($h\geqslant 3$), can be simultaneously controlled at integer multiples of π, as is the case for the second-order term, then the spectral phases $\Phi(\omega_m)$ can also satisfy the ITT condition. It is difficult to satisfy this condition using the conventional approach, which

employs a single dispersive material. However, if we introduce different types of dispersive materials corresponding to the term number of the high-order dispersions to be considered, then in principle, the ITT condition can be satisfied again.

In this new approach, the extended-ITT method, the coefficients, $\phi^{(p)}$, in Equation (2), are determined by fitting the refractive indices at the respective longitudinal modes, $n(\omega_m)$, with a fourth-order polynomial in each dispersive material. Namely, if we consider the spectral phases only at the discrete longitudinal modes, then even if we increase the spectral width, we can restrict the dispersion terms to four at most—the mode number minus one, in the case where the mode number is five. The spectral dispersion curve obtained here differs from the original one while still giving us the correct phase values at the longitudinal modes. Equation (3) represents the relationship that satisfies the ITT condition in the case where the fourth-order dispersion term is the highest, and three different species of dispersive material (thicknesses: x_1, x_2, x_3) are employed:

$$\begin{cases}(\phi_1^{(2)}x_1+\phi_2^{(2)}x_2+\phi_3^{(2)}x_3)\Delta\omega^2/2!=q^{(2)}\pi\\(\phi_1^{(3)}x_1+\phi_2^{(3)}x_2+\phi_3^{(3)}x_3)\Delta\omega^3/3!=q^{(3)}\pi\\(\phi_1^{(4)}x_1+\phi_2^{(4)}x_2+\phi_3^{(4)}x_3)\Delta\omega^4/4!=q^{(4)}\pi\end{cases} \qquad (3)$$

The subscripts indicate the types of the dispersive materials that are employed, and the $q^{(p)}$ values are arbitrary integers.

In practice, we studied the case employing three materials—borate glass (BK7), silica glass, and calcite crystal (extraordinary axis) (Figure 1a). When we set the integers in Equation (3) to $q^{(2)}=21$, $q^{(3)}=2$ and $q^{(4)}=0$, we obtain material thicknesses of $x_{FS}=1.367$ mm, $x_{BK7}=1.075$ mm and $x_{Calcite}=0.179$ mm. Figure 1b displays the spectral phases realized for the second (thin line), third (dashed line) and fourth (dashed and dotted line) orders. The spectral phases at all of the longitudinal modes are controlled to integer multiples of π for each of the dispersion-order terms; thus, the ITT condition is satisfied for the total of the spectral phases, $\Phi(\omega_m)$.

To clarify the precision required for the material lengths, we fixed two of the material lengths at $x_{BK7}=1.075$ mm and $x_{Calcite}=0.179$ mm, and we plotted the peak values of the normalized waveform, $I(t)=\left|\sum^m A_m\exp[i\{\omega_m t-\Phi(\omega_m)\}]\right|^2 / I_{TL}$, as a function of the thickness, x_{FS} (Figure 1c, upper panel). A_m and I_{TL} are the spectral amplitude and the peak intensity to be obtained under the TL condition, respectively. Assuming the practical ITT condition to be $\max[I(t)]>0.99$, then this condition is satisfied for a range of $x_{FS}=1.367\pm0.006$ mm. In reality, this is a sufficiently controllable range.

To better understand the mechanism of this extended ITT, we also plotted variations in the peak intensities of the waveforms in the lower panel of figure 1c. Each dispersion-order term is included alone. The ITT condition for each dispersion-order term appears with its own periodic cycle. The solution in Equation (3) is realized when all the periodic cycles coincide ($x_{FS}=1.367$ mm). Figure 1d is a pulsed waveform obtained under this condition. A TL pulse train with a duration of 1.82 fs and an interval of 8.06 fs is produced (red curve in Figure 1d; the peak shift is due to the first-order term.)

This example shows that the extended-ITT method can be successfully applied to arbitrary initial spectral phases; moreover, the condition that completely satisfies the TL conditions can be analytically determined. One of the curious findings here is that as shown in this typical example, the extended-ITT method can function in reverse as a simple technique that employs a few thin dispersive materials for such

ultrabroad bandwidth (greater than several hundred THz) that the high-order dispersion terms are as dominant as the second-order term.

Numerical exploration method

If we increase the longitudinal-mode number further, it is also possible to produce an attosecond pulse train. However, as we increase the mode number, we run into increasing difficulty: the species of dispersive materials must be increased correspondingly, and the thicknesses required tend to be unrealistic. Next, we describe the second method, which is more practical and has the potential to give a shorter pulse duration. This method is technically similar to the extended-ITT method (Figure 1a), and this method also simply places one or more dispersive materials in the optical path. Here, however, we abandon the attempt to obtain an exact TL condition, and we numerically explore options that approximately satisfy the TL condition by randomly changing the thicknesses of the dispersive materials (numerical exploration of pulse compression (NEC)). Surprisingly, we find many such conditions within a realistic range. This method is very similar to the approach used in the extended-ITT method, but it differs essentially in terms of its physics.

As a typical example, we discuss a discrete spectrum consisting of nine longitudinal modes (bandwidth: $2\pi \times 992$ THz; see Figure 3b). To understand the basic nature of this method, we first placed only a single dispersive material (silica glass) on the optical axis. We then studied the behavior of the waveform produced as we continuously changed the thickness of the material, x_{FS}. Unexpectedly, even though we introduced only a single dispersive material, the peak intensities were recovered at more than 90% of the values under the TL condition and appeared four times in a thickness range of 30 mm (Figure 2a; arrows: 93.1% at 25.461 mm).

If we further increase the number of species used as dispersive materials, the control freedom increases correspondingly; thus, we can naturally expect to find conditions nearer to the TL. We subjected three dispersive materials—silica glass, sapphire crystal (ordinary axis), and calcium fluoride crystal—to the process described above and explored the optimum conditions by randomly changing the thicknesses of the materials (Figure 2b). In this exploration, we used 'the random search method' for numerical optimization. For the target function, we used the peak value of the normalized waveform produced. Here, $\Phi(\omega_m) = \{x_{FS} n_{FS}(\omega_m) + x_{Sa} n_{Sa}(\omega_m) + x_{CaF_2} n_{CaF_2}(\omega_m)\}\omega_m/c$. In the cubic volume of $(12 \text{ mm})^3$ set for the exploration, we found many thickness parameters that gave peak intensities of more than 90% of the intensities under the TL condition. We mapped the points or regions, or both, that had especially high values (Figure 2b). (The inset depicts an optimum region around condition III, appearing as an oblong shape of $3.18 \mu m \times 883 \mu m$.) As expected, the peak intensities approached the TL condition (unity) more closely as we introduced more species as dispersive materials. With I (one material), we obtained 0.922 for $x_{FS} = 8.254$ mm; with II (two materials), we obtained 0.979 for $x_{FS} = 10.652$ mm and $x_{Sa} = 5.312$ mm; and with III (three materials), we obtained 0.995 for $x_{FS} = 10.937$ mm, $x_{Sa} = 3.042$ mm and $x_{CaF_2} = 10.781$ mm.

If we had applied the first approach (the extended-ITT method) to the above case, seven species of dispersive material would have been necessary. The point of the second approach is that if we abandon to obtain an exact TL condition we are able to realize a pulse train that nearly satisfied the TL condition by using a more practical technique of simply adjusting a few thin dispersive materials even for many spectral modes with an ultrabroad bandwidth. In addition, this second approach to the optimum conditions can be established routinely as a numerical exploration method.
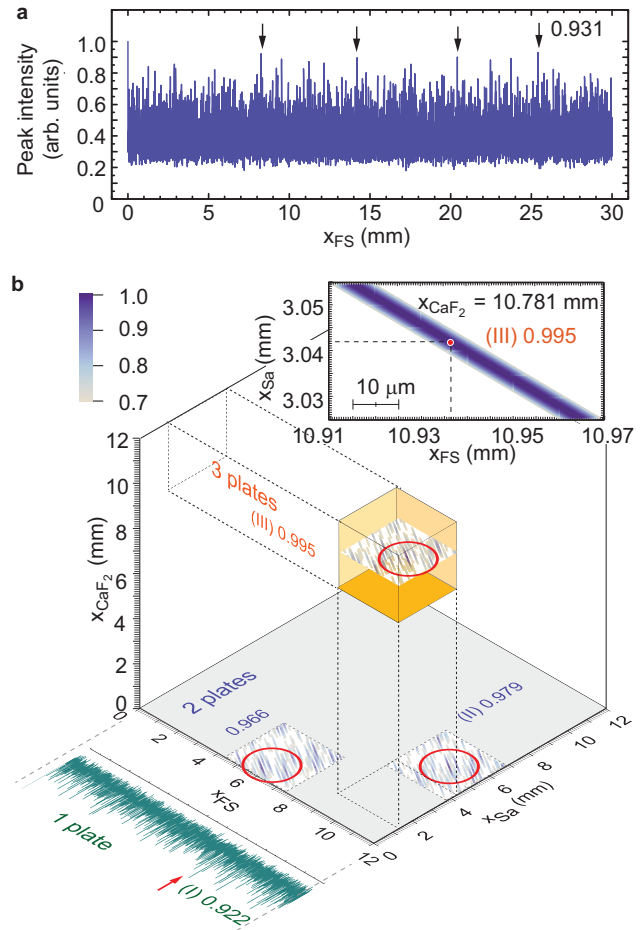

Figure 2 Exploration of optimum solutions using the NEC method. (**a**) Peak variation in the intensity waveforms as a function of the thickness of the fused-silica-glass plate. (**b**) The optimum solutions found using the NEC method for the three cases of (I) one plate, (II) two plates and (III) three plates.

Figure 3 shows that this second method differs essentially from the extended-ITT method in terms of its physical nature. Neither of the high-order dispersions under optimum condition III in Figure 2b satisfies the ITT condition. Nonetheless, their total almost realizes a linear relationship, so their deviations from the ITT conditions cancel each other out. The situation in which the bandwidth is ultrabroad results in the substantial inclusion of many dispersion-order terms, which can then function in reverse to cancel each other out. Figure 3c shows the pulsed waveform produced. An attosecond pulse train with a pulse duration equivalent to the duration under the TL condition (846 as) was produced on the basis of this numerical exploration of the optimum conditions. This method is very robust. It yields essentially the same result as if we had assumed arbitrary spectral phases initially or employed other dispersive materials.

When we examine a discrete spectrum of which the carrier-envelope offset frequency is controlled,[34–38] we can simultaneously manipulate the carrier-envelope phase in addition to the intensity waveform.[37,38] Figure 3d demonstrates that the electric field is manipulated to sine-like ($-1.0 \mu m$) or cosine-like ($+1.6 \mu m$) monocycle waveforms by slightly shifting the thickness of the silica glass employed in the NEC method from condition III.
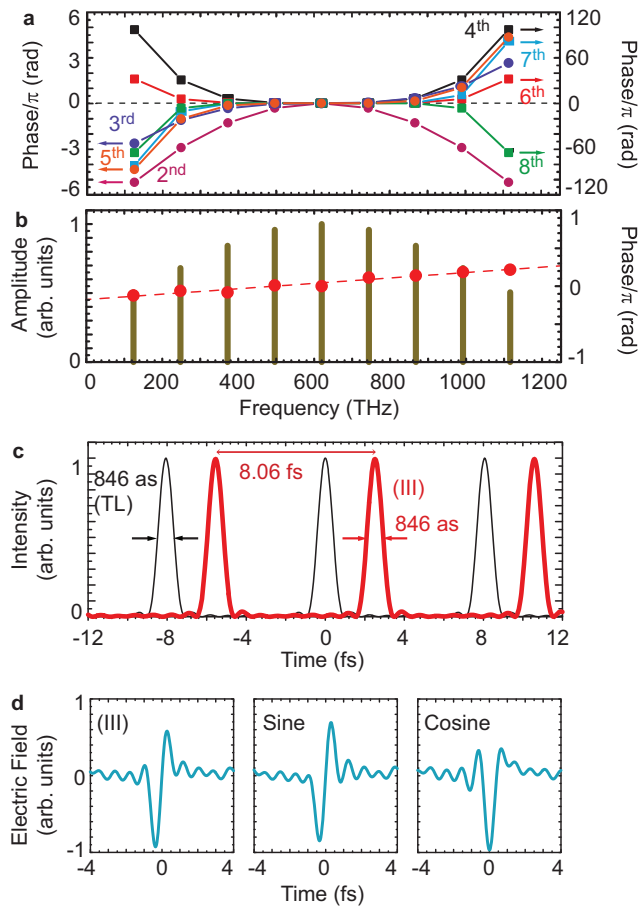
Figure 3 Attosecond pulse generation by applying the NEC method. (**a**) Spectral phases in the respective dispersion orders under the optimum condition III in Figure 2b. (**b**) The total spectral phase and the power spectrum. (**c**) The temporal intensity waveform (thick line) achieved. (**d**) Manipulation of the electrical amplitude waveforms around condition III.

Figure 4 Numerical experiment for attosecond pulse generation in an actual system (gaseous parahydrogen). (**a**) Schematic illustration of the setup and the Raman sideband generation scheme. (**b**) Power spectrum of the 12 Raman sidebands generated and their phases (i) before (blue circles) and (ii) after applying the NEC method (red dots). (**c**) The temporal intensity waveforms obtained.

RESULTS AND DISCUSSION

Lastly, we demonstrated the generation of an attosecond pulse train by executing a numerical experiment in an actual system. We generated an ultrabroad coherent discrete spectrum (frequency spacing: 124.5713 THz; bandwidth: $2\pi \times 1.4$ PHz for 12 modes, 200.5494 nm to 2.406633 μm) by adiabatically driving the pure-vibrational Raman transition (see the scheme in Figure 4a; $v=1\leftarrow0$: 124.5710 THz) in gaseous parahydrogen (5.38×10^{19} cm^{-3}; interaction length: 5 cm).[43] The excitation intensity was 5.0 GW cm^{-2}, and the two driving-laser fields, Ω_{-1} and Ω_0, were set to 622.8541 THz (481.3205 nm) and 747.4257 THz (401.1000 nm), respectively; their difference was detuned by -300 MHz from the Raman resonance. This numerical experiment was performed by operating a code based on the Maxwell–Bloch equation in the far-off resonant Λ scheme.[26–28] Figure 4b shows a generated discrete spectrum consisting of 12 modes and their spectral phases (blue circles) after the 5-mm-thick silica window and the 3-mm-thick collimating lens.

Next, we tried to produce an attosecond pulse train by controlling this ultrabroad discrete spectrum. For spectral phase control, we adopted the NEC method. We employed three species of dispersive materials—silica glass, sapphire crystal (ordinary axis), and calcium fluoride crystal. Their thicknesses were set to $x_{FS}=1.747$ mm,

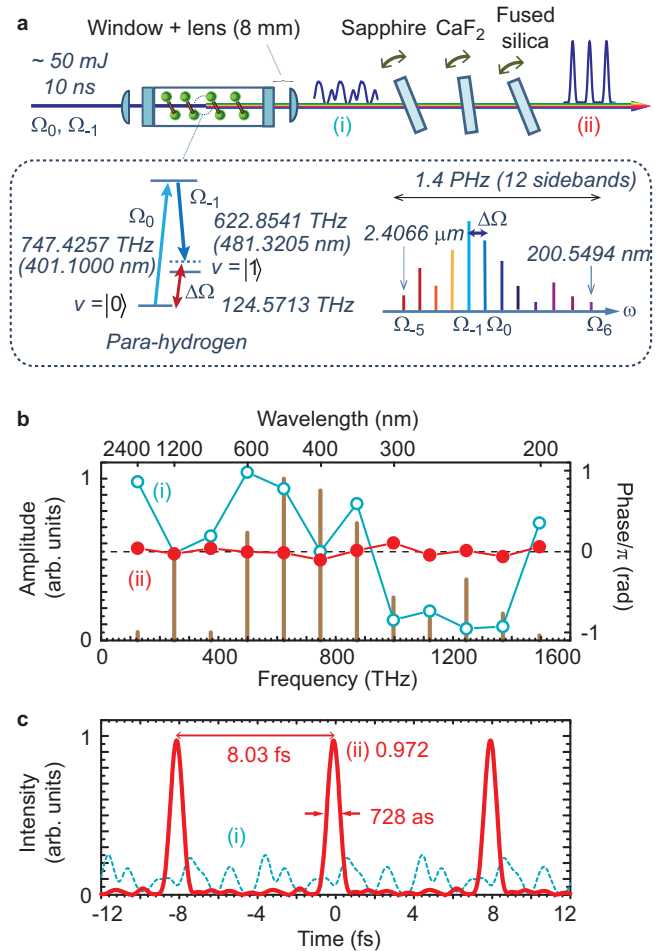$x_{Sa}=1.556$ mm and $x_{CaF_2}=3.727$ mm, respectively; these values were obtained as optimal parameters through numerical exploration.

We show the spectral phase (Figure 4b, dots) and the intensity waveform (Figure 4c, thick red line) achieved under these conditions. An attosecond pulse train with a pulse duration of 728.4 as (very near the TL pulse duration of 728.1 as) was recovered from the initial noise-burst waveform (Figure 4c, dotted line). The peak intensity was 97.2% of the intensity under the TL condition. The pulsed energy overlapping with the TL intensity waveform was estimated to be 91%. Here, we should note the transmittances of the three materials inserted. The 12 modes expand over an extremely wide spectral range of 200 nm to 2.4 μm, and therefore, the inserted materials are not perfectly transparent throughout the spectral range. However, the required thicknesses are as much as several millimeters, as estimated above, so the losses are still not significant: the transmittances of the silica glass, the calcium fluoride crystal, and the sapphire crystal plates are higher than 90%, 90% and 80% for the whole spectral range (200 nm to 2.4 μm), respectively. We have therefore demonstrated that this method could function in an actual, practical system.

In this numerical experiment, we used two single-frequency nano-second pulses (linewidth: approximately 30 MHz) to generate the

ultrabroad coherent discrete spectrum. A similar ultrabroad coherent spectrum but with much broader linewidth than tens of MHz can be also generated by simultaneously introducing a short pulse laser as a third laser.[30] This method for producing an attosecond pulse train is also applicable for an ultrabroad coherent spectrum consisting of broad-linewidth discrete modes. The application of the method is limited by the group velocity delays produced in the inserted dispersive materials.

CONCLUSIONS

In summary, we discovered two novel ways of producing a train of attosecond pulses. One method extends the ITT concept to include high-order dispersions and generates a pulse train that completely satisfies the TL conditions. The other method numerically explores the optimum conditions under which we can obtain a pulse train that approximately satisfies the TL conditions; this method is simpler and more practical than the first one. Furthermore, we performed a numerical experiment in a real gaseous parahydrogen system, where a train of attosecond pulses was generated with a TL pulse duration of 728 as through the adiabatic driving of the fundamental vibrational Raman transition. The attosecond pulse-generation methods described here are extremely simple, requiring the placement of only a few thin dispersive materials and the adjustment of their thicknesses. The methods can be applied robustly to a wide variety of systems and are attractive in their potential to be adapted for use with high-powered lasers.

1　Brabec T, Krausz F. Intense few cycle light pulses: frontiers of nonlinear optics. *Rev Mod Phys* 2000; **72**: 545–591.
2　Corkum PB, Krausz F. Attosecond science. *Nat Phys* 2007; **3**: 381–387.
3　Paul PM, Toma ES, Breger P, Mullot G, Auge F *et al*. Observation of a train of attosecond pulses from high harmonic generation. *Science* 2001; **292**: 1689–1692.
4　Hentschel M, Klenberger R, Spielmann Ch, Reider GA, Milosevic N *et al*. Attosecond metrology. *Nature* 2001; **414**: 509–513.
5　Kienberger R, Goulielmakis E, Uiberacker M, Baltuska A, Yakovlev V *et al*. Atomic transient recorder. *Nature* 2004; **427**: 817–821.
6　Sansone G, Benedetti E, Calegari F, Vozzi C, Avaldi L *et al*. Isolated single-cycle attosecond pulses. *Science* 2006; **314**: 443–446.
7　Goulielmakis E, Schultze M, Hofstetter M, Yakovlev VS, Gagnon J *et al*. Single-cycle nonlinear optics. *Science* 2008; **320**: 1614–1617.
8　Midorikawa K, Nabekawa Y, Suda A. XUV multiphoton processes with intense high-order harmonics. *Prog Quant Electron* 2008; **32**: 43–88.
9　Sola IJ, Mevel E, Elouga L, Constant E, Strelkov V *et al*. Controlling attosecond electron dynamics by phase-stabilized polarization gating. *Nat Phys* 2006; **2**: 319–322.
10　Skantzakis E, Tzallas P, Kruse J, Kalpouzos C, Charalambidis. Coherent continuum extreme ultraviolet radiation in the sub-100-nJ range generated by a high-power many-cycle laser field. *Opt Lett* 2009; **34**: 1732–1734.
11　Ferrari F, Calegari F, Lucchini M, Vozzi C, Stagira S *et al*. High-energy isolated attosecond pulses generated by above-saturation few-cycle fields. *Nat Photon* 2010; **4**: 875–879.
12　Mashiko H, Gilbertson S, Chini M, Feng X, Yun C *et al*. Extreme ultraviolet supercontinua supporting pulse durations of less than one atomic unit of time. *Opt Lett* 2009; **34**: 3337–3339.
13　Drescher M, Hentschel M, Kienberger R, Uiberacker M, Yakovlev V *et al*. Time-resolved atomic inner-shell spectroscopy. *Nature* 2002; **419**: 803–807.
14　Uiberacker M, Uphues Th, Schultze M, Verhoef AJ, Yakovlev V *et al*. Attosecond real-time observation of electron tunnelling in atoms. *Nature* 2007; **446**: 627–632.
15　Schultze M, Fieß M, Karpowicz N, Gagnon J, Korbman M *et al*. Delay in photoemission. *Science* 2010; **328**: 1658–1662.
16　Mauritsson J, Remetter T, Swoboda M, Klünder K, L'Huillier A *et al*. Attosecond electron spectroscopy using a novel interferometric pump-probe technique. *Phys Rev Lett* 2010; **105**: 053001.
17　Goulielmakis E, Loh ZH, Wirth A, Santra R, Rohringer N *et al*. Real-time observation of valence electron motion. *Nature* 2010; **466**: 739–743.
18　Eckle P, Pfeiffer AN, Cirelli C, Staudte A, Dörner R *et al*. Attosecond ionization and tunneling delay time measurements in helium. *Science* 2008; **322**: 1525–1529.
19　Kling MF, Siedschlag Ch, Verhoef AJ, Khan JI, Schultze M *et al*. Control of electron localization in molecular dissociation. *Science* 2006; **312**: 246–248.
20　Sansone G, Kelkensberg F, Torres JFP, Morales F, Kling MF *et al*. Electron localization following attosecond molecular photoionization. *Nature* 2010; **465**: 763–766.
21　Sansone G, Poletto L, Nisoli M. High-energy attosecond light sources. *Nat Photon* 2011; **5**: 655–663.
22　Sekikawa T, Kosuge A, Kanai T, Watanabe S. Nonlinear optics in the extreme ultraviolet. *Nature* 2004; **432**: 605–608.
23　Nabekawa Y, Shimizu T, Okino T, Furusawa K, Hasegawa H *et al*. Interferometric autocorrelation of an attosecond pulse train in the single-cycle regime. *Phys Rev Lett* 2006; **97**: 153904.
24　Del'Haye P, Schliesser A, Arcizet O, Wilken T, Holzwarth R *et al*. Optical frequency comb generation from a monolithic microresonator. *Nature* 2007; **450**: 1214–1217.
25　Kippenberg TJ, Holzwarth R, Diddams SA. Microresonator-based optical frequency combs. *Science* 2011; **332**: 555–559.
26　Harris SE, Sokolov AV. Broadband spectral generation with refractive index control. *Phys Rev A* 1997; **55**: R4019–R4022.
27　Harris SE, Sokolov AV. Subfemtosecond pulse generation by molecular modulation. *Phys Rev Lett* 1998; **81**: 2894–2897.
28　Kien FL, Liang JQ, Katsuragawa M, Ohtsuki K, Hakuta K *et al*. Subfemtosecond pulse generation with molecular coherence control in stimulated Raman scattering. *Phys Rev A* 1999; **60**: 1562–1571.
29　Sokolov AV, Walker DR, Yavuz DD, Yin GY, Harris SE. Raman generation by phased and antiphased molecular states. *Phys Rev Lett* 2000; **85**: 562–565.
30　Liang JQ, Katsuragawa M, Fam LK, Hakuta K. Sideband generation using strongly driven Raman coherence in solid hydrogen. *Phys Rev Lett* 2000; **85**: 2474–2478.
31　Yavuz DD, Walker DR, Shverdin MY, Yin GY, Harris SE. Quasiperiodic Raman technique for ultrashort pulse generation. *Phys Rev Lett* 2005; **91**: 233602–233605.
32　Shverdin MY, Walker DR, Yavuz DD, Yin GY, Harris SE. Generation of a single-cycle optical pulse. *Phys Rev Lett* 2005; **94**: 033904–033907.
33　Katsuragawa M, Yokoyama K, Onose T, Misawa K. Generation of a 10.6-THz ultrahigh-repetition-rate train by synthesizing phase-coherent Raman-sidebands. *Opt Exp* 2005; **13**: 5628–5634.
34　Suzuki T, Hirai M, Katsuragawa M. Octave-spanning Raman comb with carrier envelope offset control. *Phys Rev Lett* 2008; **101**: 243602-1-4.
35　Katsuragawa M, Suzuki T, Shiraga K, Arakawa M, Onose T *et al*. Ultrahigh-repetition-rate pulse train with absolute-phase control produced by an adiabatic Raman process, laser spectroscopy, Proceedings of the XIX International Conference, ICOLS; 2010. pp978–981.
36　Chen WJ, Hsieh ZM, Huang SW, Su HY, Lai CJ *et al*. Sub-single-cycle optical pulse train with constant carrier envelope phase. *Phys Rev Lett* 2008; **100**: 163906.
37　Hsieh ZM, Lai CJ, Chan HS, Wu SY, Lee CK *et al*. Controlling the carrier-envelope phase of Raman-generated periodic waveforms. *Phys Rev Lett* 2009; **102**: 213902.
38　Chan HS, Hsieh ZM, Liang WH, Kung AH, Lee CK *et al*. Synthesis and measurement of ultrafast waveforms from five discrete optical harmonics. *Science* 2011; **331**: 1165–1168.
39　Baker S, Walmsley IA, Tisch JWG, Marangos JP. Femtosecond to attosecond light pulses from a molecular modulator. *Nat Photon* 2011; **5**: 664–671.
40　Jannson T, Jannson J. Temporal self-imaging effect in single-mode fibers. *J Opt Soc Am* 1981; **71**: 1373–1376.
41　Fatome J, Pitois S, Millot G. Influence of third-order dispersion on the temporal Talbot effect. *Opt Comm* 2004; **234**: 29–34.
42　Suzuki T, Katsuragawa M. Femtosecond ultrashort pulse generation by addition of positive material dispersion. *Opt Exp* 2010; **18**: 23088–23094.
43　Suzuki M, Katsuragawa M, Sihombing RSD, Li JZ, Hakuta K. Solid hydrogen for nonlinear optics. *J Low Temp Phys* 1228; **111**: 463–468.